HHS Public Access

Author manuscript

J Biomech. Author manuscript; available in PMC 2024 May 25.

Published in final edited form as:

J Biomech. 2023 November ; 160: 111825. doi:10.1016/j.jbiomech.2023.111825.

Correlations between elastic modulus and ultrashort echo time (UTE) adiabatic T1ρ relaxation time (UTE-Adiab-T1ρ) in Achilles tendons and entheses

Saeed Jerban[1,2,3], **Amir Masoud Afsahi**[1], **Yajun Ma**[1,2], **Dina Moazamian**[1], **Sheronda Statum**[1,2], **Alecio F. Lombardi**[1,2], **Lena Kakos**[1], **Erik Dorthe**[4], **Daryll Dlima**[4], **Jiang Du**[1,2], **Christine B. Chung**[1,2], **Eric Y. Chang**[1,2]

[1]Department of Radiology, University of California, San Diego, La Jolla, CA, USA

[2]Radiology Service, Veterans Affairs San Diego Healthcare System, San Diego, La Jolla, CA, USA

[3]Department of Orthopedic Surgery, University of California, San Diego, La Jolla, CA, USA

[4]Shiley Center for Orthopedic Research and Education at Scripps Clinic, La Jolla, CA, USA

Abstract

Patients with psoriatic arthritis commonly have abnormalities of their entheses, which are the connections between tendons and bone. There are shortcomings with the use of conventional magnetic resonance imaging (MRI) sequences for the evaluation of entheses and tendons, whereas ultrashort echo time (UTE) sequences are superior for the detection of high signals, and can also be used for non-invasive quantitative assessments of these structures. The combination of UTE-MRI with an adiabatic-$T_{1\rho}$ preparation (UTE-Adiab-$T_{1\rho}$) allows for reliable assessment of entheses and tendons with decreased susceptibility to detrimental magic angle effects. This study aimed to investigate the relationship between quantitative UTE-MRI measures and the biomechanical properties of Achilles tendons and entheses. In total, 28 tendon-enthesis sections were harvested from 11 fresh-frozen human cadaveric foot-ankle specimens (52±years old). Tendon-enthesis sections were scanned using the UTE-Adiab-$T_{1\rho}$ and UTE-T_1 sequences on a clinical 3T scanner. MRI-based measures and indentation tests were performed on the enthesis, transitional, and tensile tendon zones of the specimens. Hayes' elastic modulus showed significant inverse correlations (Spearman's) with UTE-Adiab-T1ρ in all zones (R= − 0.46, − 0.54, and − 0.61 in enthesis, transition, and tensile tendon zones, respectively). Oliver-Pharr's elastic modulus showed significant inverse correlations with UTE-Adiab-T1ρ in transition (R= − 0.52) and tensile tendon zone (R=− 0.60). UTE-T_1 did not show significant correlations with the elastic modulus. UTE-MRI and elastic modulus were significantly lower in the tensile tendon compared with

Corresponding authors: Eric Y. Chang, Radiology Service, Veterans Affairs San Diego Healthcare System, 3350 La Jolla Village Drive, San Diego, CA 92161, USA, eric.chang2@va.gov, Phone: +1 858 642 1221, Fax: +1 888 960 5922; **Saeed Jerban**, Department of Radiology, University of California, 9500 Gilman Dr., San Diego, CA 92093, USA, sjerban@health.ucsd.edu, Phone: +1 858 246 2229, Fax : +1 858 246 2221.

Conflict of interest statement

The authors have no conflicts of interest to declare.

the enthesis regions This study highlights the potential of the UTE-Adiab-$T_{1\rho}$ technique for the non-invasive evaluation of tendons and entheses.

Keywords

Achilles tendon; enthesis; MRI; ultrashort echo time; mechanical properties

1. Introduction

Tendon and bone comprise a special interacting unit that is essential for locomotion and individual autonomy (Edwards et al., 2015). The enthesis, which is the region connecting tendon to bone, distributes stress over a wide area or volume. This region varies in composition depending on the location in the body, and fibrous and fibrocartilaginous entheses have been described. The structure of the enthesis also varies, both at the macroscopic and the microscopic levels, and there are significant spatial differences in collagen fiber orientation near the bone when compared with the portions closer to the tensile tendon or ligament.

Entheses are commonly involved in many diseases, including overuse syndromes as well as the early stages of osteoarthritis (OA) and seronegative spondyloarthropathies (Benjamin and Ralphs, 1998, 1997; Tan, 2006). In psoriatic arthritis (PsA), the enthesis is one of the primary targets of the disease (McGonagle, 2003; Watad et al., 2017). Noninvasive imaging is crucial for diagnosis and management, and magnetic resonance imaging (MRI) is one modality that is routinely used for the morphological evaluation of tendons and entheses (Hodgson et al., 2012; Pierre-Jerome et al., 2010; Weinreb et al., 2014). However, tendons and entheses typically demonstrate low signal-to-noise ratios due to the very short transverse relaxation times (T_2), and clinical MRI techniques can only be used for direct evaluation when the structures are markedly abnormal (Chang et al., 2015a; Du et al., 2010b; Juras et al., 2012). In contrast to conventional MRI sequences, ultrashort echo time (UTE) MRI techniques can detect considerable signals from both short- and long-T_2 components, permitting evaluation of tendons and entheses throughout the entire range of disease, from healthy to damaged (Chang et al., 2015a; Ma et al., 2022). UTE-MRI can also be used for quantitative assessment, such as through the measurement of apparent transverse relaxation time (UTE-T_2*) (Agergaard et al., 2021; Chang et al., 2015b, 2014; Chen et al., 2018b, 2018a; Filho et al., 2009; Jerban et al., 2017; Juras et al., 2012; Liu et al., 2019; Malmgaard-Clausen et al., 2021; Qiao et al., 2017; Robson et al., 2004; Xie et al., 2020), longitudinal relaxation time (UTE-T_1) (Chen et al., 2018a; Filho et al., 2009; Jerban et al., 2022b, 2019; Wright et al., 2012), longitudinal relaxation time in a rotating frame (UTE-$T_{1\rho}$) (Chen et al., 2018a; Du et al., 2010a), and magnetization transfer (MT) (Chen et al., 2018b, 2018a; Fang et al., 2022; Hodgson et al., 2011; Jerban et al., 2022b, 2019; Zhu et al., 2018).

$T_{1\rho}$ has been reported to be sensitive to proteoglycan (PG) depletion (Duvvuri et al., 2001, 1997; Li et al., 2008, 2007, 2005; Regatte et al., 2006, 2003). However, the main confounding factor is the magic angle effect (Du et al., 2009; Erickson et al., 1993;

Fullerton et al., 1985; Goodwin et al., 1998; Henkelman et al., 1994; Mlynárik et al., 2004; Mosher et al., 2001; Rubenstein et al., 1993; Shao et al., 2017; Xia et al., 1997). $T_{1\rho}$ values significantly increase when the orientation angle of the collagen fibers in the tissue approaches 55° relative to the B0 field (MRI bore direction). $T_{1\rho}$ values can vary considerably due to magic angle-related effects, with reports of 76% (Wu et al., 2020), 92% (Shao et al., 2017), 32% (Wang and Xia, 2013), and 11% (Li et al., 2011) variations, depending on the sequence that is utilized and the magnitude of the orientation angle alteration. The higher end of these $T_{1\rho}$ variations can exceed changes caused by degeneration, which are typically in the range of 10–30% (Mosher et al., 2011), thereby complicating diagnosis and treatment monitoring based on $T_{1\rho}$. Notably, UTE-$T_{1\rho}$ using a typical continuous-wave spin lock-pulse is also sensitive to the magic angle effect (Shao et al., 2017). On the contrary, employing a cluster of adiabatic inversion recovery spin-lock pulses for preparation before a 3D-UTE-Cones data acquisition (UTE-Adiab-$T_{1\rho}$) (Ma et al., 2018), can measure $T_{1\rho}$ with low sensitivity to the magic angle effect (Ma et al., 2018; Wu et al., 2020). UTE-Adiab-$T_{1\rho}$ has demonstrated significant inverse correlations with the tensile elastic modulus of the human anterior cruciate ligament (ACL) (n=13, $R=-0.59$, $p<0.01$)(Jerban et al., 2022a) as well as the indentation-based elastic modulus of tibiofemoral cartilage (n=40, $R=-0.54$ for superficial layer and $R=-0.37$ for total thickness cartilage, $p<0.01$)(Namiranian et al., 2020).

This study aimed to investigate the correlations of UTE-Adiab-$T_{1\rho}$ and UTE-T_1 with the biomechanical properties of Achilles tendons and entheses. We hypothesize that UTE-Adiab-$T_{1\rho}$ will show significant correlations with the elastic modulus of the Achilles tendon and enthesis, at a similar level to previously examined musculoskeletal tissues (ligament and articular cartilage). This study will highlight the UTE-Adiab-$T_{1\rho}$ technique for the non-invasive characterization of biomechanical properties.

2. Material and Methods

2.1. Sample preparation

Eleven fresh-frozen human cadaveric foot-ankle specimens (52±18 years old at the time of death) were provided by two whole-body donation companies (United Tissue Network, Phoenix, AZ, USA, and Medcure, Portland, OR, USA). Distal-posterior sides of the specimens were cut using a commercial bandsaw (B16, Butcher Boy Machines, Selmer, TN, USA) and a low-speed diamond saw (Isomet 1000, Buehler, IL, USA) into 4- to 6-mm thick sagittal sections including the Achilles tendon, enthesis, and the calcaneus bone. The total number of sections was 28 (2–3 sections per donor). All tendon-enthesis specimens were visually inspected and appeared grossly normal. The tendon-enthesis specimens were soaked in phosphate-buffered saline (PBS) for 2 hours to ensure adequate rehydration after potential drying throughout the sample preparation.

2.2. MRI scanning

MRI scans were performed on a 3T MRI scanner (MR750, GE Healthcare Technologies, WI, USA) using a standard GE eight-channel knee coil at room temperature. All specimens were placed in a plastic container filled with perfluoropolyether (Fomblin, Ausimont, NJ,

USA) to minimize dehydration and susceptibility artifacts during MRI scans. The container was positioned carefully inside the knee coil to ensure that the tensile sections of the tendons were perpendicular to B0. All MR images were acquired in the sagittal plane of the tendon-enthesis specimens (i.e., the axial plane in the scanner).

To measure UTE-T_1, an actual flip angle imaging-variable flip angle (AFI-VFA) sequence (AFI: TE=0.032ms, TRs=20,100ms, FA=45°; VFA: TE=0.032ms, TR=20ms, FAs=5, 10, 20, 30°) (Ma et al., 2019) was performed with a total scan time of 35 minutes. To measure UTE-Adiab-$T_{1\rho}$ values, five fat-saturated 3D-UTE-Cones sequences with adiabatic $T_{1\rho}$ preparation (Ma et al., 2018) were performed with the following parameters: TR=500 ms; FA=10°, number of spokes=25; spin-locking time (TSL)=0, 12, 24, 36, and 48ms; number of adiabatic full passage (AFP) pulses=0, 2, 4, 6, and 8. T1 and B1 maps calculated from the AFI-VFA sequence were used as prerequisites to correct the UTE-Adiab-$T_{1\rho}$ measure. The total approximate scan time for UTE-Adiab-$T_{1\rho}$ was 20 minutes. In addition to the UTE-MRI sequences, a clinical T1-weighted CUBE sequence (TR= 926 ms, TE=18 ms, and FA=90°) was performed for qualitative morphological evaluation of the specimens. Other imaging parameters for the performed sequences are summarized in Table 1.

2.3. Mechanical indentation testing

Specimens were washed with PBS after the MRI scans and were soaked in PBS for 30 minutes before mechanical tests. Skin, muscle, and fatty tissues were gently removed using a scalpel before performing mechanical tests. Indentation testing was performed using a commercial biomechanical testing system (MACH-1, Biomomentum, Quebec, Canada). The specimens were placed in 2-inch square Petri dishes filled with PBS to avoid dehydration during the mechanical testing. A 1.0-mm diameter plane-ended cylinder indenter was positioned perpendicular to the cut surfaces of the specimens. Specimens were tested along 7–10 rows of points depending on the size of the specimens. Each row of the measurement was manually set by the operator, starting from the bone-enthesis side (1 mm apart from the bone edge) and ending at the proximal edge of the tendon. The distance between rows was 2 mm, while the distance between points in each row was 1 mm. The indenter motion within and between rows was performed by horizontal displacement of the stage in the X and Y directions, respectively, using the operating software. The schematics of the tested points are shown in Figure 1a. Points in each row were labeled based on the distance from the bone edge and the length of each row (L). Specifically, points with a distance below L/3 from bone were referred to as the enthesis zone (red points in Figure 1a), points with a distance above L/3 and below 2L/3 from bone were referred to as the transition zone (yellow points in Figure 1a), and points with a distance above 2L/3 from bone were referred to as the tensile tendon zone (blue points in Figure 1a).

Figure 1b shows the indentation test setup measuring the mechanical properties of a representative Achilles tendon-enthesis specimen. After finding the contact between the indenter tip and the tissue, the actuator lowered the indenter at a rate of 100 μm/sec. The loading was followed by immediate unloading with an unloading rate of 100 μm/sec. Maximum indentation depth was set at 300 μm (<10% of the minimum thickness of the specimens) in order to avoid significant nonlinearities in the tissue deformation.

The average mechanical properties for each point were measured from two consecutive indentation processes, with five seconds of rest time in between. Figure 1c shows the load-displacement curve for a representative indentation test (two consecutive indentations) to measure maximum load (P_{max}), which is required for the calculation of Hayes elastic modulus (E_{Hayes}) using Eq. 1 (Hayes et al., 1972). The unloading slope (S) of the load-displacement curve was used for required for the calculation of Oliver-Pharr's elastic modulus ($E_{Oliver\text{-}Pharr}$) (Delaine-Smith et al., 2016; Oliver and Pharr, 1992), which is recommended for nonlinear materials and soft tissues. Overlaying the load-displacement curves for the two consecutive indentations illustrated a high repeatability level in the mechanical measurement process.

$$E_{Hayes} = \frac{\left(1-\upsilon^2\right)}{2ak}\frac{P_{max}}{depth} \quad \text{Eq. 1}$$

$$E_{\text{Oliver-Pharr}} = \frac{S}{2a} \quad \text{Eq. 2}$$

where ν, a, Pmax, S, depth, and k are Poisson's ratio, the radius of the indenter, maximum load, unloading slope, indentation depth, and correction factor (k=1.25) introduced by Hayes et al. (Hayes et al., 1972), respectively. The correction factor selection was based on the provided chart in Hayes et al. (Hayes et al., 1972) study, which utilizes the indenter diameter, indentation depth, and Poisson's ratio to guide the selection. A Poisson's ratio of 0.45 was used in the calculations, which was expected to be appropriate as the loading rate was assumed to be relatively fast, and only a limited outward water flux was expected to occur in the meantime (Delaine-Smith et al., 2016).

2.4. MRI data analysis

Sections with MRI artifacts due to metal particles and air bubbles present around the specimens were excluded. In total, three enthesis zone sections, one transition zone section, and one tensile tendon zone section were excluded. Finally, 25, 27, and 27 datasets were used for enthesis, transition, and tensile tendon zone evaluations, respectively.

UTE-T_1 and UTE-Adiab-$T_{1\rho}$ were calculated in a representative midsagittal slice for each specimen (Figure 1a) for 3×3-pixel regions of interest (ROIs). The center of each square ROI was selected visually by an experienced analyst to be matched with the indentation points, which are schematically illustrated in Figure 1a. Recorded pictures of the indentation points were used to ensure a rigorous ROI selection process. Single-component exponential fitting models (Eq.3 and Eq.4) were used to measure UTE-T_1 and UTE-Adiab-$T_{1\rho}$ relaxation times.

$$\mathrm{I(FA)} = M_0 sin(B_1 . FA)\frac{1-exp(-\mathrm{TR}/T_1)}{1-exp(-\mathrm{TR}/T_1)\cos(B_1 . FA)} + constant \quad [9]$$

Eq. 3

$$I(TSL) = M_0 \sin(B_1 . FA) \frac{\exp\left(-\frac{TSL}{T_{1\rho}}\right).\left(1-\exp\left(-\frac{TR-TSL}{T_1}\right)\right)}{1-\exp\left(-\frac{TSL}{T_{1\rho}}\right).\exp\left(-\frac{TR-TSL}{T_1}\right).\cos(B_1 . FA)} + constant$$

Eq. 4

Where I, M0, B1, FA, and TR refer to the mean signal intensity, equilibrium magnetization, RF field magnitude, and nominal flip angle.

2.5. Statistical analysis

Since a perfect co-localization between indentation points and MRI ROIs was not possible, for each studied tendon-enthesis specimen (n=28 from 11 donors), arithmetic means of the MRI and indentation results within the enthesis, transition, and tensile tendon zones were used for statistical analysis. The one-sample Kolmogorov-Smirnov test determined that the MRI and indentation results were not normally distributed. Therefore, Spearman's rank correlations were calculated between the mean UTE MRI quantifications (UTE-T1 and UTE-Adiab-T1ρ) and measured mechanical properties (peak indentation load and Hayes's and Oliver-Pharr's elastic modulus). To ensure that intra-specimen dependency does not affect the results. All correlation studies have been repeated using one average measure per donor. As an exploratory study, the Kruskal-Wallis test by ranks was used to examine the differences between the MRI and mechanical measures in enthesis, transition, and tensile tendon zones. P-values < 0.05 were considered significant. The Holm-Bonferroni method was used to correct the significance level for multiple comparisons between groups. All UTE MRI measurements and statistical analyses were performed using MATLAB (version 2021, The Mathworks Inc., Natick, MA, USA).

3. Results

Figure 2 shows a representative Achilles tendon-enthesis specimen imaged at 3T using clinical T_1-weighted CUBE and 3D-UTE-Cones (Figure 2b) sequences. The tendon and enthesis demonstrated no detectable signals on the clinical MR image (Figure 2a), while they showed high signals when imaged with 3D-UTE-Cones (Figure 2b). The abundant signal enabled UTE-T_1 and UTE-Adiab-$T_{1\rho}$ quantifications in the targeted tissues. Pixel maps of UTE-T_1 and UTE-Adiab-$T_{1\rho}$ generated over the tendon and enthesis regions are shown in Figures 2c and 2d, respectively.

The average, standard deviation, and range of the UTE MRI quantifications and the indentation test results averaged within enthesis, transition, tensile tendon, and all zones are presented in Table 2.

Table 3 presents Spearman's correlation coefficients between elastic modulus (Hayes's and Oliver-Pharr's) and UTE-MRI measures. Correlation coefficients are calculated for averaged variables per section (n=28) and per donor (n=11). Hayes' elastic modulus showed significant inverse correlations with UTE-Adiab-T1ρ in all zones (R= − 0.46, − 0.54, and

− 0.61 in enthesis, transition, and tensile tendon zones, respectively). Oliver-Pharr's elastic modulus showed a significant inverse correlation with UTE-Adiab-T1ρ only in transition (R= − 0.52) and tensile tendon zone (R=− 0.60). When averaged per donor, the UTE-Adiab-T1ρ correlations with elastic modulus were found to be significant only in the tensile tendon zone (R= − 0.79 and − 0.74 for Hayes's and Oliver-Pharr's elastic modulus, respectively). Correlations between UTE-T1 and elastic modulus were insignificant.

Figures 3 and 4 show the scatter plots and linear trendlines of Hayes's and Oliver-Pharr's elastic modulus versus UTE-Adiab-$T_{1\rho}$ for averaged results per section and per donor, respectively.

The mean UTE-MRI and indentation differences between the enthesis, transition, and tensile tendon zones are presented in Table 4. The mean UTE-T_1, UTE-Adiab-$T_{1\rho}$, and Hayes's and Oliver-Pharr's elastic modulus were significantly lower in the tensile tendon zone compared with the enthesis ($p<0.01$ using the Kruskal-Wallis test). Mean measures in the transition zone were lower than the enthesis zone but higher than the tensile tendon zone. However, the differences were not statistically significant, except for the UTE-T1 difference between the tensile and transition zones.

4. Discussion

This study investigated the correlation between quantitative UTE-MRI measures (UTE-Adiab-$T_{1\rho}$ and UTE-T_1) with indentation-based biomechanical properties of Achilles tendons and entheses. Significant correlations were found between UTE-Adiab-$T_{1\rho}$ values and elastic moduli in the enthesis, transition, and tensile tendon zones. These findings, in addition to the reported low sensitivity to the magic angle effect (Ma et al., 2018; Wu et al., 2020), highlight the UTE-Adiab-$T_{1\rho}$ technique as a useful tool for enthesis and tendon assessment.

Prior studies employing conventional, continuous-wave $T_{1\rho}$ techniques have shown inverse correlations between $T_{1\rho}$ values and macromolecular contents, particularly PG in cartilage (Jobke et al., 2013; Nishioka et al., 2012). The significant negative correlations between UTE-Adiab-$T_{1\rho}$ and the mechanical properties of the entheses and tendons observed in this study are consistent with the prior results, as PG content is known to maintain tissue swelling pressure as a result of the negative charges on the molecule, which attract sodium and water(Maroudas et al., 1969). It should be noted that the relationship between UTE-Adiab-$T_{1\rho}$ and PG/collagen content in entheses and tendons is yet to be investigated by comparing with the histological and biochemical ground truth measures. In addition, the strength of the correlations between UTE-Adiab-$T_{1\rho}$ values and tissue elastic moduli (R=0.46–0.61) was in the range of the previously reported UTE-Adiab-$T_{1\rho}$ correlations with the elastic moduli of ACL samples (R=0.60) (Jerban et al., 2022a) and tibiofemoral cartilage (R=0.33–0.54) (Namiranian et al., 2020).

We found higher UTE-T1, UTE-Adiab-T1ρ, and elastic modulus values in the enthesis zones compared with the tensile tendon zones. Higher UTE-T1 values in the enthesis zones also agreed with the results from previous investigations (Chen et al., 2018a). Notably,

UTE-Adiab-T1ρ values for Achilles tendons and entheses have not yet been reported in the literature. Chen et al. (Chen et al., 2018a) used quantitative UTE measures and found higher UTE-T_2* yet lower magnetization transfer (MT) ratio values in the enthesis compared with the tensile tendon zones (Chen et al., 2018a). The range of the elastic modulus values obtained in this study differed from the previous study (Chen et al., 2018a), likely due to variations in indentation devices and mechanical testing parameters, including indenter shape, indenter diameter, indentation depth, and loading rate.

The limitations of this study can be summarized in six aspects. First, the number of samples was relatively small (28 sections from 11 donors), as is the nature of pilot ex vivo studies using rigorous reference standards. Moreover, the tendon-enthesis specimens were from eleven donors without any visible abnormality such as degeneration or tearing. The inclusion of more tendon-enthesis specimens with various degrees of degeneration would increase the generalizability of this study. Second, the elastic modulus measurement on the studied specimens was performed using indentation tests by lateral compression forces. Though this does not mimic the in vivo forces over the main length of the tendons, which is typically exposed to tensile loading, enthesis units do course around the calcaneus during dorsiflexion and plantarflexion of the ankle resulting in compression forces (Benjamin et al., 2006; Benjamin and Ralphs, 1998). Moreover, entheses and nearby tendon regions may include fibrocartilage differentiation from tendon cells involving changes in cell shape and expression of cartilage markers, especially type II collagen, and aggrecan (Benjamin et al., 2006; Benjamin and Ralphs, 1998). Third, the limited spaces between indentation points (i.e., 1–2mm) might result in high dependency between the original data points. However, since arithmetic means of the MRI and indentation results within the larger zones (enthesis, transition, and tensile tendon) were used for statistical analysis, the net effect would likely have minimal influence on the results. Fourth, the tendon and its enthesis are viscoelastic and nonlinear materials that may not be well examined using elastic modulus alone. The viscoelastic properties of the tissue might lead to insufficient recovery of the tested points before indenting the neighboring points. Also, using a lower Poisson's ratio (<0.45) may be appropriate in future experiments because the assumption of a fast indentation with limited minor outward water flux during the loading in this study can be challenged. Although, the ratio between the tissue thickness and the indentation depth was higher than 10, assuming a zero-radial displacement at the interface of the tissue and Petri dish is challenging, which might result in Pmax underestimation. Future investigations should consider performing mechanical stress-relaxation and creep experiments on well-secured specimens to be compared with the quantitative MRI biomarkers. Fifth, specimens were soaked in PBS for 2 hours before scanning to ensure similar rehydration levels, which may affect the quantitative MRI measures and indentation results. However, the impact of the PBS soaking was assumed to be similar in all specimens and did not influence the comparisons presented in this study. Sixth, the long scan time of the proposed technique may limit its translation to clinical studies. Employing acceleration techniques (53), using less TSL points for T1ρ fitting, and utilizing reasonable constant values for T1 (excluding the T1 acquisition with ~20 minutes of scan time) could reduce the scan time to near 10 minutes for future in vivo investigations.

5. Conclusion

Correlations between UTE-Adiab-$T_{1\rho}$ and indentation-based elastic modulus of Achilles tendons and entheses were investigated and were found to be significant in the enthesis, transition, and tensile tendon zones. This study highlights the potential of the UTE-Adiab-$T_{1\rho}$ technique, which is known to be less sensitive to magic angle effects, for the non-invasive characterization of biomechanical properties in tendons and entheses.

Acknowledgements

The authors acknowledge grant support from the National Institutes of Health (R01AR075825, K01AR080257, R01AR068987, R01AR062581, R01AR079484, and 5P30AR073761), Veterans Affairs Clinical Science and Rehabilitation R&D (I01CX001388, I01BX005952, and I01CX000625), and GE Healthcare.

References

Agergaard A-S, Malmgaard-Clausen NM, Svensson RB, Nybing JD, Boesen M, Kjaer M, Magnusson SP, Hansen P, 2021. UTE T2* mapping of tendinopathic patellar tendons: an MRI reproducibility study. Acta radiol 62, 215–224. 10.1177/0284185120918807 [PubMed: 32340475]

Benjamin M, Ralphs JR, 1998. Fibrocartilage in tendons and ligaments--an adaptation to compressive load. J Anat 193 (Pt 4, 481–494. 10.1046/j.1469-7580.1998.19340481.x [PubMed: 10029181]

Benjamin M, Ralphs JR, 1997. Tendons and ligaments--an overview. Histol Histopathol 12, 1135–1144. [PubMed: 9302572]

Benjamin M, Toumi H, Ralphs JR, Bydder G, Best TM, Milz S, 2006. Where tendons and ligaments meet bone: attachment sites ('entheses') in relation to exercise and/or mechanical load. J Anat 208, 471–490. 10.1111/j.1469-7580.2006.00540.x [PubMed: 16637873]

Chang EY, Du J, Bae WC, Statum S, Chung CB, 2014. Effects of Achilles tendon immersion in saline and perfluorochemicals on T2 and T2*. Journal of Magnetic Resonance Imaging 40, 496–500. 10.1002/jmri.24360 [PubMed: 24155129]

Chang EY, Du J, Chung CB, 2015a. UTE imaging in the musculoskeletal system. Journal of Magnetic Resonance Imaging 41, 870–883. 10.1002/jmri.24713 [PubMed: 25045018]

Chang EY, Du J, Iwasaki K, Biswas R, Statum S, He Q, Bae WC, Chung CB, 2015b. Single- and Bi-component T2Star analysis of tendon before and during tensile loading, using UTE sequences. Journal of Magnetic Resonance Imaging 42, 114–120. 10.1002/jmri.24758 [PubMed: 25223714]

Chen B, Cheng X, Dorthe EW, Zhao Y, Bydder GM, Liu S, Du J, Ma Y-J, Ya-Jun Ma C, 2018a. Evaluation of normal cadaveric Achilles tendon and enthesis with ultrashort echo time (UTE) magnetic resonance imaging and indentation testing. 10.1002/nbm.4034

Chen B, Zhao Y, Cheng X, Ma Y, Chang EY, Kavanaugh A, Liu S, Du J, 2018b. Three-dimensional ultrashort echo time cones (3D UTE-Cones) magnetic resonance imaging of entheses and tendons. Magn Reson Imaging 49, 4–9. 10.1016/j.mri.2017.12.034 [PubMed: 29309823]

Delaine-Smith RM, Burney S, Balkwill FR, Knight MM, 2016. Experimental validation of a flat punch indentation methodology calibrated against unconfined compression tests for determination of soft tissue biomechanics. J Mech Behav Biomed Mater 60, 401–415. 10.1016/j.jmbbm.2016.02.019 [PubMed: 26974584]

Du J, Carl M, Diaz E, Takahashi A, Han E, Szeverenyi NM, Chung CB, Bydder GM, 2010a. Ultrashort TE T1rho (UTE T1rho) imaging of the Achilles tendon and meniscus. Magn Reson Med 64, 834–842. 10.1002/mrm.22474 [PubMed: 20535810]

Du J, Chiang AJT, Chung CB, Statum S, Znamirowski R, Takahashi A, Bydder GM, 2010b. Orientational analysis of the Achilles tendon and enthesis using an ultrashort echo time spectroscopic imaging sequence. Magn Reson Imaging 28, 178–184. 10.1016/j.mri.2009.06.002 [PubMed: 19695811]

Du J, Pak BC, Znamirowski R, Statum S, Takahashi A, Chung CB, Bydder GM, 2009. Magic angle effect in magnetic resonance imaging of the Achilles tendon and enthesis. Magn Reson Imaging 27, 557–564. 10.1016/j.mri.2008.09.003 [PubMed: 19022600]

Duvvuri U, Charagundla SR, Kudchodkar SB, Kaufman JH, Kneeland JB, Rizi R, Leigh JS, Reddy R, 2001. Human Knee: In Vivo T1ρ-weighted MR Imaging at 1.5 T—Preliminary Experience. Radiology 220, 822–826. 10.1148/radiol.2203001662 [PubMed: 11526288]

Duvvuri U, Reddy R, Patel SD, Kaufman JH, Kneeland JB, Leigh JS, 1997. T1ρ-relaxation in articular cartilage: Effects of enzymatic degradation. Magn Reson Med 38, 863–867. 10.1002/mrm.1910380602 [PubMed: 9402184]

Edwards MH, Dennison EM, Aihie Sayer A, Fielding R, Cooper C, 2015. Osteoporosis and sarcopenia in older age. Bone 80, 126–130. 10.1016/j.bone.2015.04.016 [PubMed: 25886902]

Erickson SJ, Prost RW, Timins ME, 1993. The “magic angle” effect: background physics and clinical relevance. Radiology 188, 23–25. 10.1148/radiology.188.1.7685531 [PubMed: 7685531]

Fang Y, Zhu D, Wu W, Yu W, Li S, Ma Y-J, 2022. Assessment of Achilles Tendon Changes After Long-Distance Running Using Ultrashort Echo Time Magnetization Transfer MR Imaging. 10.1002/jmri.28072

Filho GH, Du J, Pak BC, Statum S, Znamorowski R, Haghighi P, Bydder G, Chung CB, 2009. Quantitative characterization of the achilles tendon in cadaveric specimens: Tl and T2* measurements using ultrashort-TE MRI at 3 T. American Journal of Roentgenology 192, 117–124. 10.2214/AJR.07.3990 [PubMed: 19098189]

Fullerton GD, Cameron IL, Ord VA, 1985. Orientation of tendons in the magnetic field and its effect on T2 relaxation times. Radiology 155, 433–435. 10.1148/radiology.155.2.3983395 [PubMed: 3983395]

Goodwin DW, Wadghiri YZ, Dunn JF, 1998. Micro-imaging of articular cartilage: T2, proton density, and the magic angle effect. Acad Radiol 5, 790–798. 10.1016/s1076-6332(98)80264-x [PubMed: 9809078]

Hayes WC, Keer LM, Herrmann G, Mockros LF, 1972. A mathematical analysis tests of articular cartilage. J Biomech 5, 541–551. [PubMed: 4667277]

Henkelman RM, Stanisz GJ, Kim JK, Bronskill MJ, 1994. Anisotropy of NMR properties of tissues. Magn Reson Med 32, 592–601. 10.1002/mrm.1910320508 [PubMed: 7808260]

Hodgson R, O’Connor PJ, Grainger AJ, 2012. Tendon and ligament imaging. British Journal of Radiology 85, 1157–1172. 10.1259/bjr/34786470 [PubMed: 22553301]

Hodgson RJ, Evans R, Wright P, Grainger AJ, O’connor PJ, Helliwell P, Mcgonagle D, Emery P, Robson MD, 2011. Quantitative magnetization transfer ultrashort echo time imaging of the Achilles tendon. Magn Reson Med 65, 1372–1376. 10.1002/mrm.22715 [PubMed: 21500263]

Jerban S, Hananouchi T, Ma Y, Namiranian B, Dorthe EW, Wong JH, Shojaeiadib N, Wu M, Du J, D’Lima D, Chung CB, Chang EY, 2022a. Correlation between the elastic modulus of anterior cruciate ligament (ACL) and quantitative ultrashort echo time (UTE) magnetic resonance imaging. J Orthop Res. 10.1002/jor.25266

Jerban S, Ma Y, Afsahi AM, Lombardi A, Wei Z, Shen M, Wu M, Le N, Chang DG, Chung CB, Du J, Chang EY, 2022b. Lower Macromolecular Content in Tendons of Female Patients with Osteoporosis versus Patients with Osteopenia Detected by Ultrashort Echo Time (UTE) MRI. Diagnostics 12, 1061. 10.3390/diagnostics12051061 [PubMed: 35626217]

Jerban S, Ma Y, Namiranian B, Ashir A, Shirazian H, Zhao W, Wu M, Cai Z, Le N, Du J, Chang EYEY, Wei Z, Le N, Wu M, Cai Z, Du J, Chang EYEY, 2019. Age-related decrease in collagen proton fraction in tibial tendons estimated by magnetization transfer modeling of ultrashort echo time magnetic resonance imaging (UTE-MRI). Sci Rep November, 17974. 10.1038/s41598-019-54559-3

Jerban S, Nazaran A, Cheng X, Carl M, Szeverenyi N, Du J, Chang EY, 2017. Ultrashort echo time T2* values decrease in tendons with application of static tensile loads. J Biomech 61, 160–167. 10.1016/j.jbiomech.2017.07.018 [PubMed: 28780188]

Jobke B, Bolbos R, Saadat E, Cheng J, Li X, Majumdar S, 2013. Mechanism of disease in early osteoarthritis: Application of modern MR imaging techniques - a technical report. Magn Reson Imaging 31, 156–161. 10.1016/j.mri.2012.07.005 [PubMed: 22902064]

Juras V, Zbyn S, Pressl C, Valkovic L, Szomolanyi P, Frollo I, Trattnig S, 2012. Regional variations of T2* in healthy and pathologic achilles tendon in vivo at 7 Tesla: Preliminary results. Magn Reson Med 68, 1607–1613. 10.1002/mrm.24136 [PubMed: 22851221]

Li X, Benjamin Ma C, Link TM, Castillo D-D, Blumenkrantz G, Lozano J, Carballido-Gamio J, Ries M, Majumdar S, 2007. In vivo T1ρ and T2 mapping of articular cartilage in osteoarthritis of the knee using 3T MRI. Osteoarthritis Cartilage 15, 789–797. 10.1016/j.joca.2007.01.011 [PubMed: 17307365]

Li X, Cheng J, Lin K, Saadat E, Bolbos RI, Jobke B, Ries MD, Horvai A, Link TM, Majumdar S, 2011. Quantitative MRI using T1ρ and T2 in human osteoarthritic cartilage specimens: Correlation with biochemical measurements and histology. Magn Reson Imaging 29, 324–334. 10.1016/j.mri.2010.09.004 [PubMed: 21130590]

Li X, Han ET, Busse RF, Majumdar S, 2008. In vivoT1ρ mapping in cartilage using 3D magnetization-prepared angle-modulated partitionedk-space spoiled gradient echo snapshots (3D MAPSS). Magn Reson Med 59, 298–307. 10.1002/mrm.21414 [PubMed: 18228578]

Li X, Han ET, Ma CB, Link TM, Newitt DC, Majumdar S, 2005. In vivo 3T spiral imaging based multi-slice T1ρ mapping of knee cartilage in osteoarthritis. Magn Reson Med 54, 929–936. 10.1002/mrm.20609 [PubMed: 16155867]

Liu J, Nazaran A, Ma Y, Chen H, Zhu Y, Du J, Li S, Zhou Q, Zhao Y, 2019. Single- and Bicomponent Analyses of T2 * Relaxation in Knee Tendon and Ligament by Using 3D Ultrashort Echo Time Cones (UTE Cones) Magnetic Resonance Imaging. Biomed Res Int 2019, 1–9. 10.1155/2019/8597423

Ma Y, Carl M, Searleman A, Lu X, Chang EY, Du J, 2018. 3D adiabatic T1ρprepared ultrashort echo time cones sequence for whole knee imaging. Magn Reson Med 80, 1429–1439. 10.1002/mrm.27131 [PubMed: 29493004]

Ma Y, Jang H, Jerban S, Chang EY, Chung CB, Bydder GM, Du J, 2022. Making the invisible visible—ultrashort echo time magnetic resonance imaging: Technical developments and applications. Appl Phys Rev 9, 041303. 10.1063/5.0086459 [PubMed: 36467869]

Ma YJ, Zhao W, Wan L, Guo T, Searleman A, Jang H, Chang EY, Du J, 2019. Whole knee joint T1 values measured in vivo at 3T by combined 3D ultrashort echo time cones actual flip angle and variable flip angle methods. Magn Reson Med 81, 1634–1644. 10.1002/mrm.27510 [PubMed: 30443925]

Malmgaard-Clausen NM, Jørgensen OH, Høffner R, Andersen PEB, Svensson RB, Hansen P, Nybing JD, Magnusson SP, Kjær M, 2021. No Additive Clinical or Physiological Effects of Short-term Anti-inflammatory Treatment to Physical Rehabilitation in the Early Phase of Human Achilles Tendinopathy: A Randomized Controlled Trial. Am J Sports Med 49, 1711–1720. 10.1177/0363546521991903 [PubMed: 33719579]

Maroudas A, Muir H, Wingham J, 1969. The correlation of fixed negative charge with glycosaminoglycan content of human articular cartilage. Biochimica et Biophysica Acta (BBA) - General Subjects 177, 492–500. 10.1016/0304-4165(69)90311-0 [PubMed: 4239606]

McGonagle D, 2003. Diagnosis and treatment of enthesitis. Rheum Dis Clin North Am 29, 549–560. 10.1016/s0889-857x(03)00044-9 [PubMed: 12951867]

Mlynárik V, Szomolányi P, Toffanin R, Vittur F, Trattnig S, 2004. Transverse relaxation mechanisms in articular cartilage. Journal of Magnetic Resonance 169, 300–307. 10.1016/j.jmr.2004.05.003 [PubMed: 15261626]

Mosher TJ, Smith H, Dardzinski BJ, Schmithorst VJ, Smith MB, 2001. MR Imaging and T2 Mapping of Femoral Cartilage. American Journal of Roentgenology 177, 665–669. 10.2214/ajr.177.3.1770665 [PubMed: 11517068]

Mosher TJ, Zhang Z, Reddy R, Boudhar S, Milestone BN, Morrison WB, Kwoh CK, Eckstein F, Witschey WRT, Borthakur A, 2011. Knee Articular Cartilage Damage in Osteoarthritis: Analysis of MR Image Biomarker Reproducibility in ACRIN-PA 4001 Multicenter Trial. Radiology 258, 832–842. 10.1148/radiol.10101174 [PubMed: 21212364]

Namiranian B, Jerban S, Ma Y, Dorthe EW, Masoud-Afsahi A, Wong JH, Zhao W, Wei Z, Chen Y, D'Lima D, Chang EY, Du J, 2020. Assessment of mechanical properties of articular cartilage with quantitative three-dimensional ultrashort echo time (UTE) Cones magnetic resonance imaging. J Biomech In Press. 10.1016/j.jbiomech.2020.110085

Nishioka H, Hirose J, Nakamura E, Oniki Y, Takada K, Yamashita Y, Mizuta H, 2012. T 1ρ and T 2 mapping reveal the in vivo extracellular matrix of articular cartilage. Journal of Magnetic Resonance Imaging 35, 147–155. 10.1002/jmri.22811 [PubMed: 21990043]

Oliver WC, Pharr GM, 1992. An improved technique for determining hardness and elastic modulus using load and displacement sensing indentation experiments. J Mater Res 7, 1564–1583. 10.1557/JMR.1992.1564

Pierre-Jerome C, Moncayo V, Terk MR, 2010. MRI of the Achilles tendon: a comprehensive review of the anatomy, biomechanics, and imaging of overuse tendinopathies. Acta radiol 51, 438–454. 10.3109/02841851003627809 [PubMed: 20380605]

Qiao Y, Tao H-Y, Ma K, Wu Z-Y, Qu J-X, Chen S, 2017. UTE-T2 * Analysis of Diseased and Healthy Achilles Tendons and Correlation with Clinical Score: An In Vivo Preliminary Study. 10.1155/2017/2729807

Regatte RR, Akella SVS, Borthakur A, Kneeland JB, Reddy R, 2003. In Vivo Proton MR Three-dimensional T1ρ Mapping of Human Articular Cartilage: Initial Experience. Radiology 229, 269–274. 10.1148/radiol.2291021041 [PubMed: 14519880]

Regatte RR, Akella SVS, Lonner JH, Kneeland JB, Reddy R, 2006. T1ρ relaxation mapping in human osteoarthritis (OA) cartilage: Comparison of T1ρ with T2. Journal of Magnetic Resonance Imaging 23, 547–553. 10.1002/jmri.20536 [PubMed: 16523468]

Robson MD, Benjamin M, Gishen P, Bydder GM, 2004. Magnetic resonance imaging of the Achilles tendon using ultrashort TE (UTE) pulse sequences. Clin Radiol 59, 727–735. 10.1016/j.crad.2003.11.021 [PubMed: 15262548]

Rubenstein JD, Kim JK, Morova-Protzner I, Stanchev PL, Henkelman RM, 1993. Effects of collagen orientation on MR imaging characteristics of bovine articular cartilage. Radiology 188, 219–226. 10.1148/radiology.188.1.8511302 [PubMed: 8511302]

Shao H, Pauli C, Li S, Ma Y, Tadros AS, Kavanaugh A, Chang EY, Tang G, Du J, 2017. Magic angle effect plays a major role in both T1rho and T2 relaxation in articular cartilage. Osteoarthritis Cartilage 25, 2022–2030. 10.1016/j.joca.2017.01.013 [PubMed: 28161394]

Tan AL, 2006. Combined high-resolution magnetic resonance imaging and histological examination to explore the role of ligaments and tendons in the phenotypic expression of early hand osteoarthritis. Ann Rheum Dis 65, 1267–1272. 10.1136/ard.2005.050112 [PubMed: 16627540]

Wang N, Xia Y, 2013. Experimental Issues in the Measurement of Multi-component Relaxation Times in Articular Cartilage by Microscopic MRI Nian. Journal of Magnetic Resonance 235, 15–25. 10.1016/j.jmr.2013.07.001.Experimental [PubMed: 23916991]

Watad A, Eshed I, McGonagle D, 2017. Lessons Learned from Imaging on Enthesitis in Psoriatic Arthritis. Isr Med Assoc J 19, 708–711. [PubMed: 29185286]

Weinreb JH, Sheth C, Apostolakos J, McCarthy M-BB, Barden B, Cote MP, Mazzocca AD, 2014. Tendon structure, disease, and imaging. Muscles Ligaments Tendons J 4, 66–73. 10.32098/mltj.01.2014.12 [PubMed: 24932450]

Wright P, Jellus V, McGonagle D, Robson M, Ridgeway J, Hodgson R, 2012. Comparison of two ultrashort echo time sequences for the quantification of T 1 within phantom and human Achilles tendon at 3 T. Magn Reson Med 68, 1279–1284. 10.1002/mrm.24130 [PubMed: 22246857]

Wu M, Ma Y, Kasibhatla A, Chen M, Jang H, Jerban S, Chang EY, Du J, 2020. Convincing evidence for magic angle less-sensitive quantitative T 1ρ imaging of articular cartilage using the 3D ultrashort echo time cones adiabatic T 1ρ (3D UTE cones-AdiabT 1ρ) sequence. Magn Reson Med 1, 1–8. 10.1002/mrm.28317

Xia Y, Farquhar T, Burton-Wurster N, Lust G, 1997. Origin of cartilage laminae in MRI. Journal of Magnetic Resonance Imaging 7, 887–894. 10.1002/jmri.1880070518 [PubMed: 9307916]

Xie Y, Liu S, Qu J, Wu P, Tao H, Chen S, 2020. Quantitative Magnetic Resonance Imaging UTE-T2* Mapping of Tendon Healing After Arthroscopic Rotator Cuff Repair: A Longitudinal Study. Am J Sports Med 48, 2677–2685. 10.1177/0363546520946772 [PubMed: 32813550]

Zhu Y, Cheng X, Ma Y, Wong JH, Xie Y, Du J, Chang EY, 2018. Rotator cuff tendon assessment using magic-angle insensitive 3D ultrashort echo time cones magnetization transfer (UTE-Cones-MT) imaging and modeling with histological correlation. Journal of Magnetic Resonance Imaging 48, 160–168. 10.1002/jmri.25914 [PubMed: 29219218]

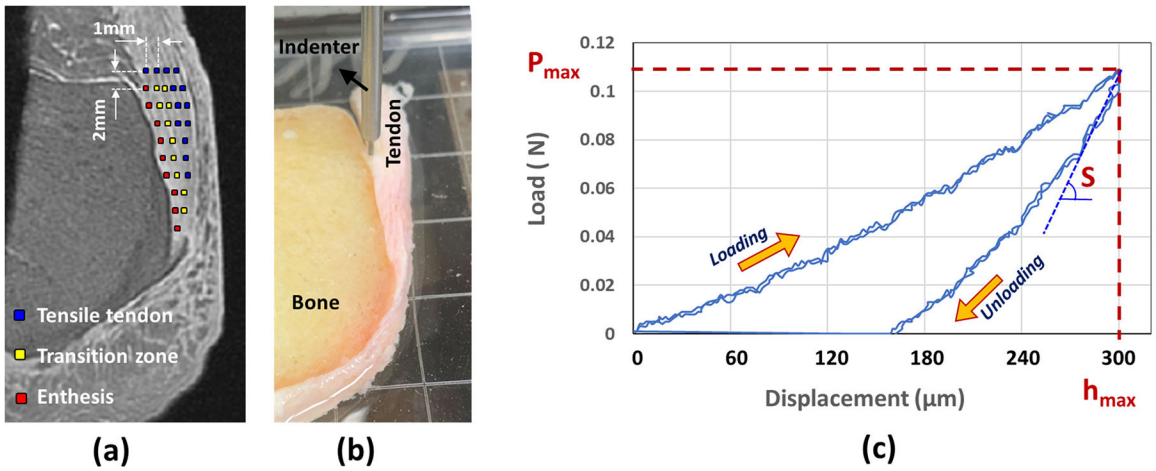

Figure 1.

(a) The schematics of the tested points on a representative Achilles tendon-enthesis specimen using indentation testing. Tested points are shown on a UTE-MRI image. (b) Experimental setup for indentation test performed on a representative Achilles tendon-enthesis specimen using a commercial biomechanical testing system (MACH-1; Biomomentum, Quebec, Canada) and a 1.0-mm diameter plane-ended cylinder indenter. Specimens were tested along 7–10 rows of points, each starting from the enthesis side and ending at the edge of the tendon. Points were manually set by an operator and labeled based on the distance from the bone edge with enthesis (distance below L/3 from bone, L is the length of each row, red points), transition (distance above L/3 and below 2L/3 from bone, yellow points), or tensile tendon (distance above 2L/3) zones. (c) Load-displacement curve indicating the loading and unloading processes at a displacement rate of 100µm/s (maximum indentation depth was 300 µm > 1/10 of the average specimen thickness). Overlaying load-displacement curves for two indentation processes showed the high repeatability level of the mechanical measurement. P_{max} and S refer to the maximum load and unloading slope required for the calculation of Hayes's of Oliver-Pharr's elastic modulus.

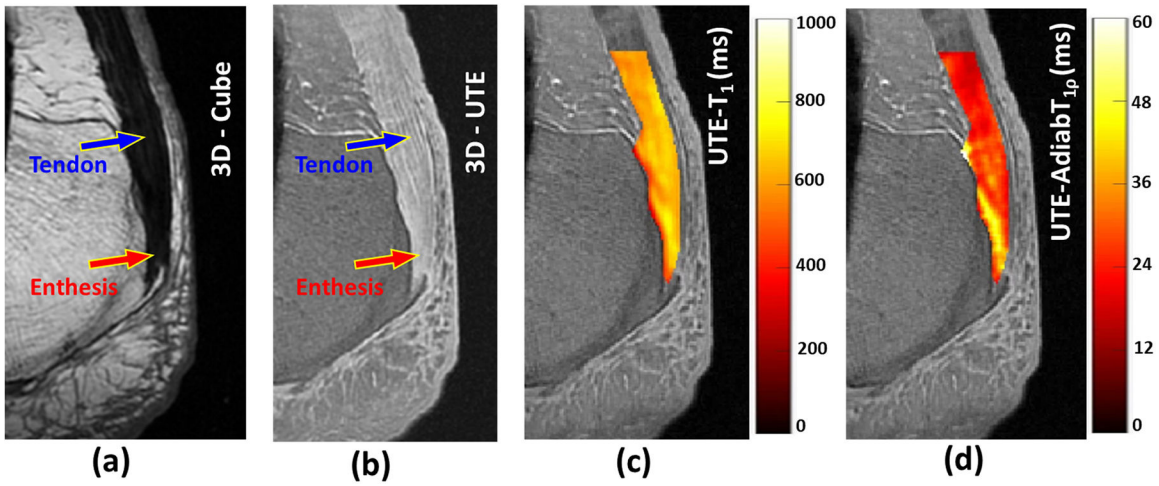

Figure 2:

(a) A representative Achilles tendon-enthesis specimen imaged at 3T using a clinical T_1-weighted CUBE sequence (TR= 926 ms, TE=18 ms) where the tendon (blue arrow) and enthesis (red arrow) demonstrated no detectable signals. (b) UTE MRI (TR= 500 ms, TE=0.032ms) image of the same specimen with high signal acquired for both the tendon (blue arrow) and enthesis (red arrow). (c) Overlayed UTE-T_1 and UTE-Adiab-$T_{1\rho}$ pixel maps within the tensile tendon and enthesis regions.

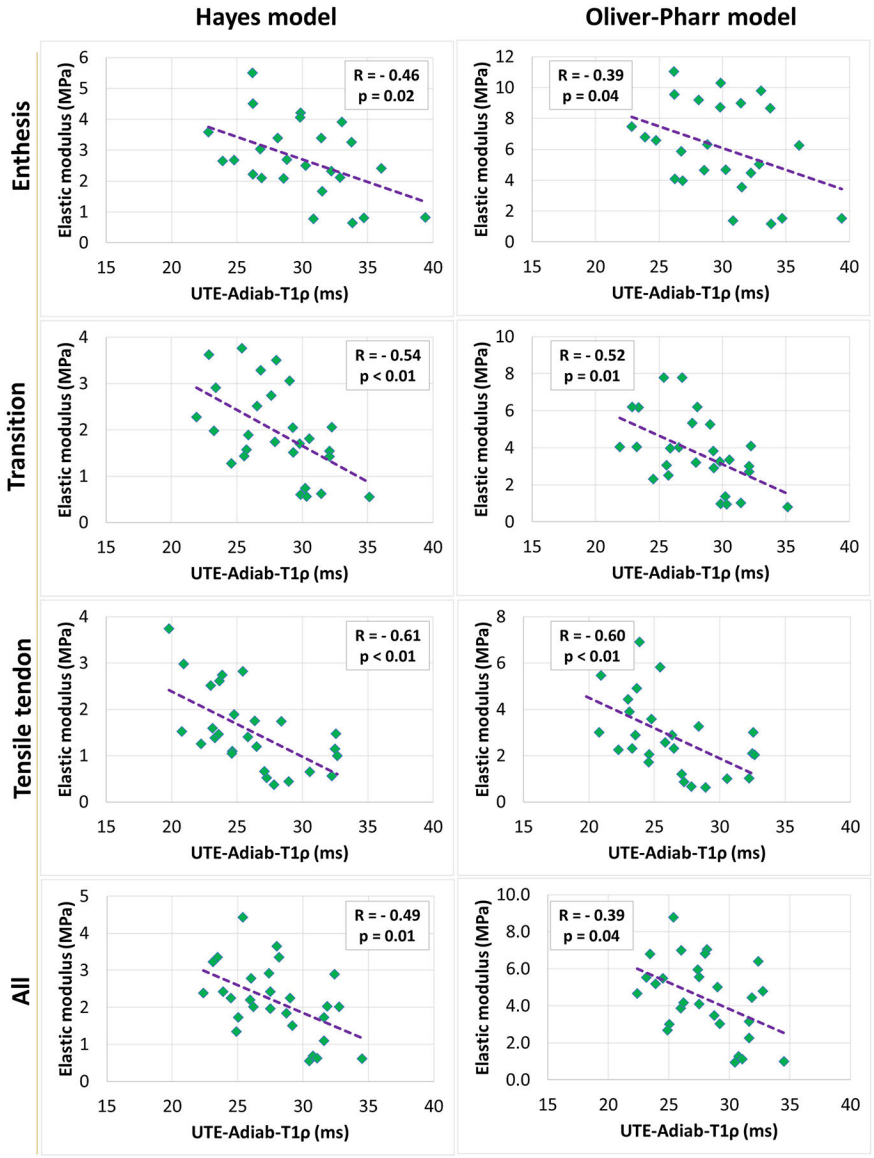

Figure 3:

Scatterplots and linear trendlines of Hayes's and Oliver-Pharr's elastic modulus versus UTE-Adiab-$T_{1\rho}$ values for averaged variables per section. R referred to Spearman's correlation coefficient.

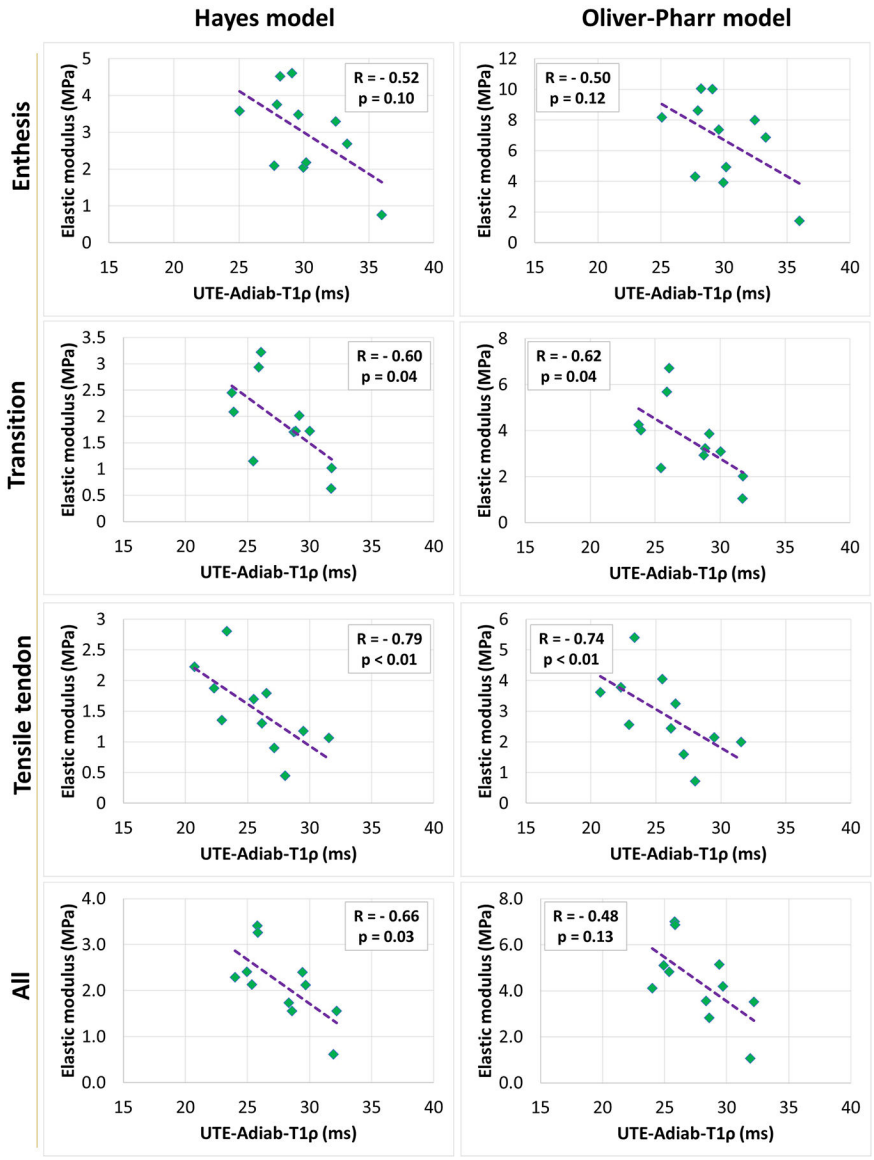

Figure 4:

Scatterplots and linear trendlines of Hayes's and Oliver-Pharr's elastic modulus versus UTE-Adiab-$T_{1\rho}$ values for averaged variables per donor. R referred to Spearman's correlation coefficient.

Table 1:

Summarized MRI sequence parameters

Sequence	TRs/TEs/TSL (ms); FA (°)	Scan time (min)	Other parameters
AFI-VFA 3D-UTE-Cones T_1	AFI: TE=0.032; TRs=20 and 100; FA=45; VFA: TE=0.032; TR=20; FAs=5, 10, 20, 30;	35	• FOV = 110 mm^2 • Matrix = 340×340 • In-plane pixel size = 0.32×0.32 mm^2 • Band width = 125 kHz • Slice thickness = 0.8 mm • Number of slices = 100 (cover all specimens in one scan)
Fat-saturated 3D-UTE-Cones Adiab-$T_{1\rho}$	TR=500; TSL=0, 12, 24, 36, and 48; FA=10;	20	
Clinical T_1-weighted CUBE	TR=926; TE=18; FA=90;	5	

Table 2:

The average, standard deviation (SD), and ranges of UTE-MRI measures and indentation test results (n=28).

	UTE-T_1 (ms)	UTE-Adiab-$T_{1\rho}$ (ms)	Peak load (N)	Hayes Elastic modulus (MPa)	Oliver-Pharr Elastic modulus (MPa)	
Enthesis	829±75 [696–953]	30.0±3.9 [22.8–39.4]	1.27±0.57 [0.31–2.59]	2.71.0±1.21 [0.66–5.51]	6.10.0±2.92 [1.21–11.07]	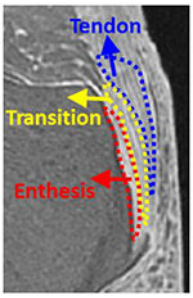
Transition	797±77 [658–932]	28.0±3.3 [21.9–35.1]	0.92±0.44 [0.26–1.78]	1.95±0.94 [0.55–3.77]	3.71±1.93 [0.79–7.79]	
Tensile tendon	735±79 [588–863]	26.0±3.7 [19.8–32.7]	0.72±0.40 [0.18–1.76]	1.54±0.85 [0.38–3.74]	2.92±1.70 [0.63–6.91]	
All	788±71 [667–918]	28.0±3.2 [22.4–34.5]	1.01±0.45 [0.26–2.09]	2.15±0.95 [0.55–4.43]	4.41±2.02 [0.95–8.77]	

Table 3:

The Spearman's correlation coefficients between elastic modulus and UTE-MRI measures. Correlation coefficients are calculated for averaged variables per section and per donor.

		Averaged data per section (n=25–27*)		Averaged data per donor (n=11)	
		UTE-T_1	**UTE-Adiab-$T_{1\rho}$**	**UTE-T_1**	**UTE-Adiab-$T_{1\rho}$**
Enthesis	**Hayes Elastic modulus**	−0.36 (p=0.07)	**−0.46 (p=0.02)**	−0.27 (p=0.42)	−0.52 (p=0.10)
	Oliver-Pharr Elastic modulus	−0.30 (p=0.15)	−0.39 (p=0.04)	−0.19 (p=0.57)	−0.50 (p=0.12)
Transition	**Hayes Elastic modulus**	−0.29 (p=0.14)	**−0.54 (p<0.01)**	−0.37 (p=0.26)	−0.60 (p=0.04)
	Oliver-Pharr Elastic modulus	−0.30 (p=0.13)	**−0.52 (p=0.01)**	−0.35 (p=0.30)	−0.62 (p=0.04)
Tensile	**Hayes Elastic modulus**	−0.34 (p=0.08)	**−0.61 (p<0.01)**	−0.38 (p=0.25)	**−0.79 (p<0.01)**
	Oliver-Pharr Elastic modulus	−0.36 (p=0.06)	**−0.60 (p<0.01)**	−0.38 (p=0.25)	**−0.74 (p=0.01)**
All	**Hayes Elastic modulus**	−0.28 (p=0.15)	**−0.49 (p=0.01)**	−0.52 (p=0.10)	−0.66 (p=0.03)
	Oliver-Pharr Elastic modulus	−0.20 (p=0.32)	−0.39 (p=0.04)	−0.36 (p=0.27)	−0.48 (p=0.13)

*n refers to the number of datapoints which was 25, 27, and 27 for enthesis, transition, and tensile tendon zones, respectively.

Table 4:

Mean UTE-MRI and indentation differences between the enthesis, transition, and tensile tendon zones. Statistical significance was examined with the Kruskal-Wallis test.

	Difference		
	Transition/Enthesis	**Tensile/Enthesis**	**Tensile/Transition**
UTE-T_1(ms)	−32 (p=0.36)	− 94 (p<0.01)	− 62 (p=0.03)
UTE-Adiab-$T_{1\rho}$(ms)	−1.9 (p=0.24)	−3.9 (p<0.01)	−2.0 (p=0.17)
Peak load (N)	−0.4 (p=0.08)	−0.5 (p<0.01)	−0.2 (p=0.25)
Hayes Elastic modulus (MPa)	−0.8 (p=0.08)	−1.2 (p<0.01)	−0.4 (p=0.25)
Oliver-Pharr Elastic modulus (MPa)	−2.4 (p=0.01)	−3.2 (p<0.01)	−0.8 (p=0.32)